Stabilization of the coupled oxygen and phosphorus cycles by the evolution of bioturbation

R.A. Boyle[1,7,*], T.W. Dahl[1,2], A.W. Dale[3], G.A. Shields-Zhou[4], M. Zhu[5], M.D. Brasier[6], D.E. Canfield[1] & T.M. Lenton[7]

[1] Institute of Biology and Nordic Centre for Earth Evolution, University of Southern Denmark

[2]Natural History Museum of Denmark, University of Copenhagen, Denmark

[3]GEOMAR Helmholtz Centre for Ocean Research, Kiel, Germany

[4]Department of Earth Sciences, University College London, UK

[5]Nanjing Institute of Geology and Palaeontology, State Key Laboratory of Palaeobiology and Stratigraphy, Nanjing, China

[6]Department of Earth Sciences, University of Oxford, UK

[7] College of Life and Environmental Sciences, University of Exeter, UK

[*]Corresponding author rboyle@biology.sdu.dk

Animal burrowing and sediment-mixing (bioturbation) began during the run up to the Ediacaran-Cambrian boundary[1,2,3], initiating a transitional interval[4,5] separating stratified Precambrian[6] from well-mixed Phanerozoic[7] sediment archetypes. This rise in bioturbation occurred in between oxygen increases at ~551 million years ago (Ma)[8,9] and ~400(Ma)[10] million years ago(Ma), whilst the global oxygen reservoir was probably smaller than present[10,11]. Phosphorus is the long-term[12] limiting nutrient for oxygen production via burial of organic carbon[13], and its retention (relative to carbon) within

organic matter in marine sediments is enhanced by bioturbation[14-17], probably in part through increased microbial polyphosphate sequestration[18]. Here we show in a simple model that introducing this link between bioturbation and organic phosphorus burial robustly triggers a net decrease in atmospheric oxygen- the magnitude of which is contingent upon the prescribed difference in C:P ratios between bioturbated and laminated sediments. Bioturbation also reduces steady state marine phosphate levels, but this effect is offset by declining Fe-adsorbed phosphate burial with lower oxygen. Dynamical model simulations show how introducing oxygen-sensitive bioturbation triggers an initial oxygen decrease, which subsequently curtails bioturbation intensity in a net negative feedback loop. This trajectory is consistent with evidence for changes in ocean oxygenation concurrent with the rise of bioturbation.

The first widely accepted trace fossil evidence for locomotion at about 565 Ma[1] is succeeded by very shallow, three dimensional burrowing from about 555 Ma[2,3]. This is followed by a diversity increase in observable bioturbation traces across the Ediacaran-Cambrian boundary,[19] e.g. from around 540 Ma burrows tend to appear in more inshore environments, and become larger and more frequently open-ended[19,20]. An emerging view of this early Cambrian "substrate revolution" suggests largely unmixed sediments in some parts of the continental shelf[5], during what was presumably a spatially heterogeneous ocean sediment system, undergoing a transitional phase involving progressive loss of sediment stratification. Nevertheless, it is clear that by ~530-525 Ma the intensity of bioturbation had increased significantly[3]. Between Cambrian stages 1 (541-~529 Ma) and 2 (~529-~521Ma), maximum burrow depth rose to almost modern levels of up to a metre, and the bioturbation index (a measure of the percentage of primary bedding fabric disrupted by bioturbation[21]) changed from 0.5 to 2.3[3], a value around which it remained around until Cambrian stage 5.

The palaeoredox context in which this biological change occurred is depicted in figure 1, which shows a compilation of U and Mo concentration and Mo isotope data,[10] compared to average and maximum bioturbation index[21,3] between 580-490 Ma. Between approximately 520 and 510 Ma, after the initial increase in the average bioturbation index, marine shale δ^{98}Mo, U and Mo content points to declining oxygen, over a time interval of around 10-15 million years. We argue this is consistent with a decrease in the size of the global oxygen reservoir immediately after the first appreciable bioturbation. It is important to emphasize the need for caution in any attempt at a quantitative reconstruction of oxygen's trajectory during this time interval, and that temporal variability is implied by existing data. For example, some data from ~499 Ma point to widespread euxinia[11], although, conversely, a pulse of oxygenation has also been suggested 1-2 million years later[22]. Nevertheless the δ^{98}Mo proxy does specifically focus on reservoir size changes[10], and does imply declining oxygen.

The earliest moving animals would, of course, have required organic carbon for food, which today is predominantly buried in continental shelf sediments[23]. Within such sediments bioturbation would have reduced stratification, and bioirrigation would have increased reactive surface area for chemical exchange with the water column. The potential significance of the impact of these sort of changes on sediment composition is illustrated by the behaviour of phosphorus. Marine shales derived from bioturbated sediments exhibit organic C:P ratios as low as 150, whereas those derived from laminated sediments can have C:P ratios of up to 3900[15], with typical values in the region of 500-700[16,24]. There are three probable mechanistic explanations[14,15] for these differences: (i) microbial polyphosphate sequestration in well-mixed sediments under oxygenated conditions[14,18], with subsequent accumulation of refractory organic P compounds; (ii) greater retention of phosphate via adsorption on Fe-oxyhydroxides[14,15] in sediments exposed to oxygenated waters by bioturbation (leading to subsequent P burial in inorganic phases); and (iii) enhanced organic

carbon preservation in anoxic and/or euxinic conditions[14] (i.e. aside from any change in P), due ultimately to the increased energy yield of aerobic respiration.

These mechanisms are already represented in existing models of the long-term coupling between the phosphorus and oxygen cycles, but redox-linked changes in modelled C:P ratios of buried organic matter are expressed as a function of the ocean anoxic fraction, rather than bioturbation[25,26]. In this work, we focus on the timing of the onset of the sensitivity of organic phosphorus burial to ocean oxygenation, making the case that this sensitivity can be attributed to bioturbation. We hypothesize that increased exposure of sediments to oxygen in overlying water, caused by bioturbation and bioirrigation, initiated an organic phosphorus sink via increased microbial polyphosphate sequestration[18] (i.e. mechanism (i) above) for the first time during the early Cambrian.

We adapted an existing model[26] (see Methods), describing the coupled long-term dynamics of the marine phosphate and nitrate reservoirs, and the oxygen content of the atmosphere (and surface ocean). The model includes a weak inverse dependence of organic carbon burial on water column O_2[13] ((iii) above), as well as the removal of phosphate with ferric iron (Fe^{3+}) oxyhydroxides[25], which ceases under anoxic conditions ((ii) above). The burial flux of marine organic phosphorus $mopb$ is related to that of marine organic carbon $mocb$ through the bioturbated fraction f_{biot} of buried organic matter, which dictates the apportioning between the low burial ratio $C:P_{biot}$ of bioturbated sediments, and the higher value of laminated sediments $C:P_{lam}$:

$$mopb = mocb \cdot \left(\frac{f_{biot}}{C:P_{biot}} + \frac{1-f_{biot}}{C:P_{lam}}\right) \quad \textbf{(1)}$$

Mathematically this is a very simple modification to existing models, but conceptually speaking, we suggest that bioturbation is more important in determining sedimentary organic

C:P burial ratios than the oxygenation state of the overlying water *per se*. For example, sediments intermittently oxygenated by bioturbation exhibit C:P ratios closer to permanently oxygenated sediments than to anoxic ones[17], whereas even under an oxygenated water column an undisturbed sediment will go anoxic within about 2.5cm of the sediment-water interface[27]. Furthermore, we suggest that even incompletely mixed sediments would have undergone an increase in propensity to support microbial P sequestration through increased bioirrigation.

Our central result is depicted by the steady state solutions shown in figure 2. Increasing the bioturbated fraction f_{biot} of buried organic matter leads to a reduction in the size of the global oxygen reservoir - across the range of potential C:P burial ratios for bioturbated and laminated sediments, and across various different bulk weathering rates. This is because increased marine organic phosphorus burial results from increasing f_{biot}. The feedback sequence giving rise to this result is illustrated in figure 3, which shows example dynamical runs in which we ran the model to steady-state with negligible bioturbation (f_{biot} =0.01), before introducing oxygen sensitive bioturbation f_{biot} =1-*anox* (where *anox* is the anoxic fraction of ocean waters (see Methods)). Bioturbation leads to increased marine organic phosphorus burial, decreasing (phosphorus-limited) new production, marine organic carbon burial, and oxygen. As oxygen drops and anoxia increases, organic carbon burial increases due to reduced remineralisation. Increased anoxia also weakens the Fe-oxyhydroxide phosphate sink, causing a secondary increase in phosphate (therefore new production and organic carbon burial). This compensating increase in phosphate as anoxia rises explains why the impact of increased f_{biot} on the phosphate reservoir is weaker than the impact on oxygen.

The differing response of the phosphate reservoir to that of oxygen is also affected by how close the system is to anoxia prior to the introduction of bioturbation. With low weathering

$W=0.5*$ present, the lower initial oxygen reservoir size means that the bioturbation-induced phosphate sink more easily increases anoxia, feeding back negatively on the Fe-P burial flux early in the simulation, and leading to the (counter-intuitive) slight net increase in deep ocean phosphate concentration. At higher weathering rates, the initial larger O_2 reservoir means a greater initial phosphate/oxygen decrease is necessary to induce anoxia, and the overall impact on the phosphate reservoir at steady state is a negative one.

The oxygen-sensitivity of bioturbation used in the dynamical runs (figure 3), causes f_{biot} to decline asymptotically due to the drop in oxygen that it initially causes, and the resultant decrease in the organic phosphate burial flux helps the system approach a new, lower steady state oxygen level (see also supplementary figure S1). This qualitative feedback sequence is robust to changes in bulk weathering, the introduction of alternative formulations for oxidative weathering and organic carbon burial (supplementary figures S2, S3), increased C:P ratio differences (S4), and expression of f_{biot} as a direct increasing function of the global oxygen reservoir (S5) (as opposed to a decreasing function of anoxia). The key point that we wish to emphasize here is that the introduction of this feedback to the Earth system occurred as a consequence of the spread of the first bioturbating animals.

Quantitative thresholds on the overall change in the global oxygen and phosphate reservoirs that likely resulted from the introduction of bioturbation, were assessed by comparing pre- and post-bioturbation steady states across a range of simulations. Figure 4 depicts the difference between the steady states with negligible bioturbation ($f_{biot}=0.01$) and with anoxia sensitive bioturbation ($f_{biot}=1-anox$), for various C:P ratio and weathering parameters. The magnitude of the decline in the oxygen reservoir scales with the difference in C:P ratios between bioturbated and laminated sediments (also see supplementary figure S4). The size of the change in atmospheric oxygen also increases with the weathering flux of phosphorus (up to ~70% of the present flux), above which anoxia (due to high productivity, rather than low

oxygen, see methods) leads to loss of Fe-P burial, limiting the potential change in phosphate that can be induced by the bioturbation-driven organic P sink.

The nature and stability of the pre-bioturbation oxygen/phosphorus steady state is an important outstanding uncertainty. A steady state with negligible bioturbation and weaker phosphate removal (i.e. higher $C:P_{lam}$ within the pre-bioturbation organic phosphorus burial flux $mopb \approx \frac{mocb}{CP_{lam}}$), entails higher oxygen, but must nevertheless remain consistent with data for appreciable anoxia[11], implying that the organic phosphorus sink cannot have been too weak, even before the onset of bioturbation (this constraint is formalised analytically in the supplemental). This means that either: (a) atmospheric oxygen remained below present levels through the latest Neoproterozoic, (with inorganic P-burial changes compensating for a high $C:P_{lam}$, keeping oxygen low), (b) there was sufficient organic P-scavenging even before bioturbation to adequately reduce $C:P_{lam}$ or (c) widespread anoxic conditions ceased with the Neoproterozoic oxygenation event (or at least were more restricted than present), only recurring much later. Intriguingly, the final possibility (c) would imply weak to negligible regulation of the oxygen reservoir (at least by ocean biogeochemistry) prior to the rise of bioturbation.

Some form of qualitative reorganisation of the global phosphorus cycle is broadly consistent with phosphorite deposition across the Precambrian-Cambrian boundary[28], perhaps linked to increased anaerobic remineralization connected to a bioturbation-induced oxygen decline (S6). However, substantial phosphorite deposition occurs well before the onset of bioturbation[28], so bioturbation cannot provide a comprehensive explanation for this phenomenon. A bioturbation-driven organic phosphorus sink is also potentially consistent with the downward trajectory of C:P ratios around 500 Ma[29], although more data is needed for the earlier Cambrian to test this supposition. Most directly, the data we present in figure 1

shows how, after the initial increase in bioturbation intensity during Cambrian stage 2, the trace element data is consistent with a drop in ocean oxygenation and a relative decrease in the size of the global oxygen reservoir.

Our results thus suggest that the earliest bioturbating animals caused a relative decline in the size of the oxygen reservoir on which they depended, initiating a net negative feedback loop through the creation of an oxygen-sensitive phosphorus sink. This strengthened the link between the oxygen and phosphorus biogeochemical cycles, and contributed to oxygen regulation across Phanerozoic time.

Methods

Redox-sensitive trace element data

Molybdenum is soluble as the molybdate MoO_4^{2-} anion in oxygenated conditions, which is removed slowly via adsorbtion onto Mn oxides. In sulphidic solutions molybdate reacts with H_2S to form reactive oxythiomolybdates $MoO4_{-x}S_x^{2-}$ that are reductively removed from solution. Distinct isotopic fractionation and burial rates are associated with (a) fully oxygenated waters, (b) low oxygen non-euxinic settings that become sulphidic at depth and (c) fully euxinic settings. All these sinks preferentially remove ^{95}Mo, but the strongest fractionation is associated with oxic settings, so that increasing seawater δ^{98}Mo indicates increasing ocean oxygenation. Because the δ^{98}Mo of euxinic shales can be lower than that of seawater, the maximum δ^{98} Mo value in shales (rather than the mean) is generally the most reliable indicator of the Mo isotopic composition of the oceans in which they were deposited. This maximum value is set by the fraction of ocean sediments that are fully oxygenated (because these oxygenated settings impart the strongest fractionation). Because Mo's residence time (today ~400 kyrs) is much longer than the mixing time of the Earth's oceans (~1.5 kyrs), seawater is well-mixed and homogenous with respect to Mo. Similarly, Uranium a has a soluble oxidised state (hexavalent U(VI), stable in oxygenated water as uranyl-tetracarbonate $UO_2(CO_3)_3^{4-}$) and an immobile reduced state (tetravalent U(IV), readily sequestered into organic rich shales in low oxygen conditions). Figure 1 shows U concentration in shales, relative to total organic carbon (which will positively correlate with ambient seawater U concentration, thus ocean oxygenation). See (for example) Dahl et al 2010[11] and Partin et al 2013[30] for detailed considerations of ancient ocean oxygenation, in relation to Mo and U respectively. We argue that the fact that a

downward trajectory in ocean oxygenation is implicit in two distinct trace elements lends weight to the possibility of a net oxygen decrease in conjunction with the rise of bioturbation.

Model

The "Redfield revisited" model by Lenton & Watson, 2000[28] (incorporating key phosphorus cycle functions by Van Capellen & Ingall 1994[27]) describes the change over time in the size of the global phosphorus PO_4 nitrate NO_3 and oxygen O_2 reservoirs:

$$\frac{dPO_4}{dt} = phosw - fepb - capb - mopb \quad \textbf{(2)}$$

$$\frac{dNO_3}{dt} = nfix - monb - denif \quad \textbf{(3)}$$

$$\frac{dO_2}{dt} = mocb - oxidw \quad \textbf{(4)}$$

Normalisation and reservoir size / concentration scaling

The total size (in moles) of the above three reservoirs is assumed to scale linearly with the average concentration (in molkg^{-1} seawater) in marine surface waters ventilating the deep ocean, via scaling factors[28] $k_{N,P} = 7.1\times10^{-22}\,kg^{-1}$ and $k_O = 8.96\times10^{-24}\,kg^{-1}$. Thus, concentrations in moles per kilogram seawater are $O_{2CONC} = O_2 \cdot k_O$ and $NO_{3CONC} = NO_3 \cdot k_{N,P}$, $PO_{4CONC} = PO_4 \cdot k_{N,P}$. Present day average surface water concentrations used for normalisation are $O_{2CONC0} = 331.5\times10^{-6}\,molkg^{-1}$, $NO_{3CONC0} = 30.9\times10^{-6}\,molkg^{-1}$, $PO_{4CONC0} = 2.2\times10^{-6}\,molkg^{-1}$, in micromoles per kilogram of seawater. Where normalised concentrations are used (denoted by an overscore) we therefore have $\overline{O_{2CONC}} = \frac{O_{2CONC}}{O_{2CONC0}}$, $\overline{NO_{3CONC}} = \frac{NO_{3CONC}}{NO_{3CONC0}}$, $\overline{PO_{4CONC}} = \frac{PO_{4CONC}}{PO_{4CONC0}}$. When normalised reservoir sizes are referred to this is relative to present day values (in moles) of $O_{20} = 3.7\times10^{19}$, $NO_{30} = 4.35\times10^{16}$, $PO_{40} = 3.1\times10^{15}$.

Fluxes

Default values for fluxes and parameters are given in tables S1 and S2 in the supplemental. *W* denotes the bulk weathering forcing relative to present. Fluxes are in units of moles per year, zero subscript denotes present day

value. Phosphorus is added to the ocean via phosphorus weathering $phosw = W \cdot phosw_0$, and removed by iron-adsorbed phosphate burial $fepb = fepb_0 (\frac{1-anox}{k_{ox}})$, (where the anoxic fraction is $anox = MAX(0, 1 - k_{ox} \cdot \overline{O_{2CONC}} \frac{newp_0}{newp})$, $k_{ox} = 0.86$ is the present day ocean's oxic fraction, and new production $newp = newp_0 \cdot MIN(117 PO_{4CONC}, \frac{117}{16} NO_{3CONC})$ in units of moles organic carbon per kilogram seawater, scales stoichiometrically with limiting nutrient concentration. Phosphorus also leaves the marine reservoir through calcium bound phosphate burial $capb = capb_0 \cdot (\frac{newp}{newp_0})^2$ and marine organic phosphorus burial $mopb = mocb \cdot (\frac{f_{biot}}{C:P_{biot}} + \frac{1-f_{biot}}{C:P_{lam}})$. Nitrate changes via nitrogen fixation $nfix = MAX(0, nfix_0 \cdot (\frac{PO_{4CONC} - \frac{NO_{3CONC}}{16}}{(PO_{4CONC0} - \frac{NO_{3CONC0}}{16})1\times10^{-6}}))$ when nitrate is deficient relative to Redfield stoichiometry with phosphate, marine organic nitrogen burial $monb = \frac{mocb}{37.5}$ and denitrification $denif = denif_0 \cdot (1 + \frac{anox}{anox_0})$, but is not directly relevant to the results discussed in this paper, beyond supporting the assumption that phosphorus is limiting over long timescales. Marine organic carbon burial $mocb = mocb_0 \cdot (\frac{newp}{newp_0})^2 \cdot De^{-BO_{2CONC}}$ (with $D = 2.127$, $B = 2277 mol^{-1} kg$) adds to the oxygen reservoir, and oxidative weathering $oxidw = oxidw_0 W$ removes from it.

This work differs from the original model by use of equation (1) in the main text and (for figures 3 & 4) by putting $f_{biot} = 1 - anox$. The model was numerically integrated in Matlab using a Runge-Kutta solver. For more detailed model description see supplementary methods and supplementary figure S7.

Analytic solutions show how simultaneous non-zero steady state oxygen and anoxia impose constraints on the scaling factor used to relate marine organic carbon and phosphorus burial

$$\frac{phosw_0 - \frac{fepb_0}{k_{ox} \cdot W} - \frac{capb_0}{f_{re\min}}}{oxidw_0} \leq \frac{f_{biot}}{C:P_{biot}} + \frac{1-f_{biot}}{C:P_{lam}} < \frac{phosw_0 - \frac{capb_0}{f_{re\min}}}{oxidw_0}$$, which can be rearranged to give maximum and minimum values for f_{biot} in terms of the C:P burial ratios, or (for a pre-bioturbation ocean), constrain the strength of the phosphorus sink in terms of $C:P_{lam}$. We also find that the partial derivative of steady state normalised oxygen with respect to the bioturbated fraction is always less than zero

$$\frac{\partial \overline{O_{2CONC}}}{\partial f_{biot}} = -\frac{W^{\frac{3}{2}} \cdot mocb_0}{fepb_0 \sqrt{f_{re\min}}} \left(\frac{1}{C:P_{biot}} - \frac{1}{C:P_{lam}}\right) < 0$$, supporting the basic result. Default flux values and derivation of analytic results are given in the supplementary methods.

References

1. Liu, A.G., McIlroy, D., & Brasier, M.D. First evidence for locomotion in the Ediacara biota from the 565 Ma Mistaken Point Formation, Newfoundland. *Geology* **38,** 123-126 (2010).
2. Menon, L., McIlroy, D. & Brasier, M.D. Evidence for Cnidaria-like behaviour in c. 560 Ma Ediacaran *Aspidella*. *Geology* **41**, 895-898. (2013).
3. Mangano, M & Buatois, L.A. Decoupling of body plan diversification and ecological structuring during the Ediacaran-Cambrian transition: Evolutionary and geobiological feedbacks. *Proc. R. Soc. B.* 281. 20140038. (2014).
4. Buatois, L.A., Narbonne, G.M., Mangano, M.G., Carmona, M.B. & Myrow, P. "Ediacaran matground persisted into the earliest Cambrian." Nature Communications 5. 3544. doi 10.1038/ncomms4544. (2014)
5. Tarhan, L.G. & Droser, M. L. Widespread delayed mixing in early to middle Cambrian marine shelfal settings. *Palaeogeo. Palaeoclim, Palaeoecol.* 399. 310-322. (2014).
6. Seilacher, A. Biomat-related lifestyles in the Precambrian. Palaios 14. 86-93 (1999).
7. Droser, M.L. & Bottjer, D.J., Trends and patterns of Phanerozoic ichnofabrics. *Ann. Rev. Earth. Planet. Sci. Lett.* **21,** 205-225 (1993).

8. Frei, R., Gaucher, C., Poulton, S.W. & Canfield, D.E. Fluctuations in Precambrian atmospheric oxygenation recorded by Chromium isotopes. *Nature* 461. 250-254. (2009).
9. Scott, C, Lyons, T.W., Bekker, A., Shen, Y., Poulton, S.W., Chu, X. & Anbar, A.D. Tracing the stepwise oxidation of the Proterozoic ocean. *Nature* **452**. 456-460. 2008.
10. Dahl, T.W., Hammarlund, E.U., Anbar, A.D., Bond, D.P.G., Hill, B.C., Gordon, G.W., Knoll, A.H., Nielsen, A.T., Schovsbo, N.H. & Canfield, D.E. Devonian rise in atmospheric oxygen correlated to the radiations in terrestrial plants and large predatory fish. *Proceedings of the National Academy of Sciences* **107,** 17911-17915 (2010).
11. Gill, B.C., Lyons, T.W., Young, S.A., Kump, L.R., Knoll, A.H. & Saltzmann M.R. Geochemical evidence for widespread euxinia in the later Cambrian ocean. *Nature* **469,** 80-83 (2011).
12. Redfield, A.C. The biological control of chemical factors in the environment. *American Scientist* **46,** 205-221 (1958).
13. Betts, J.N. & Holland, H.D. The oxygen content of ocean bottom waters, the burial efficiency of organic carbon, and the regulation of atmospheric oxygen. *Palaeogeography, Palaeoclimatology, Palaeoecology (Global and Planetary Change Section)* **97,** 5-18 (1991).
14. Ingall, E. & Jahnke, R. Evidence for enhanced phosphorus regeneration from marine sediments overlain by oxygen depleted waters. *Geochimica et Cosmochimica Acta* **58,** 2571-2575 (1994).
15. Ingall, E.D., Bustin, R.M., & Van Cappellen, P. Influence of water column anoxia on the burial and preservation of carbon and phosphorus in marine shales. *Geochimica et Cosmochimica Acta* **57,** 303-316 (1993).
16. Anderson, L.D., Delaney, M.L. & Faul, K.L. Carbon to phosphorus ratios in sediments: Implications for nutrient cycling. *Global Biogeochemical Cycles* **15,** 65-79 (2001).

17. Aller, R.C. Bioturbation and remineralization of sedimentary organic matter: effects of redox oscillation. *Chemical Geology* **114,** 331-345 (1994).

18. Kerrn-Jespersen, J.P. & Henze, M. Biological phosphorus uptake under anoxic and aerobic conditions. *Water Research.* **27,** 617-324. (1993).

19. Droser, M.L. & Bottjer, D.J. Trends in depth and extent of bioturbation in Cambrian carbonate marine environments, western United States. *Geology* **16,** 233-236 (1988).

20. McIlroy, D. & Logan, G.A. The impact of bioturbation on infaunal ecology and evolution during the Proterozoic-Cambrian transition. *Palaios* **14,** 58-72 (1999).

21. Taylor, A. Goldring, R. & Gowland, S. Analysis and application of ichnofabrics. Earth Science Reviews 60. 227-259 (2003).

22. Saltzman, M.R., Young, S.E, Kump, L.R., Gill, B.C., Lyons, T.W. & Runnegar, B. Pulse of atmospheric oxygen during the late Cambrian. *Proceedings of the National Academy of Sciences* **108,** 3876-3881 (2011).

23. Berner, R.A. 1982. Burial of organic carbon and pyrite sulphur in the modern ocean: Its Geochemical and environmental significance" Am. J. Sci. 282. 451-473.

24. Slomp, C.P., Thomson, J. & de Lange, G.J. Controls on phosphorus regeneration and burial during formation of eastern Mediterranean sapropels. *Marine Geology* **203,** 141-159 (2004).

25. Van Cappellen, P. & Ingall, E.D. Benthic phosphorus regeneration, net primary production, and ocean anoxia: A model of the coupled marine biogeochemical cycles of carbon and phosphorus. *Paleoceanography* **9,** 677-692 (1994).

26. Lenton, T.M. & Watson, A.J. Redfield revisited: 2. What regulates the oxygen content of the atmosphere? *Global Biogeochemical Cycles* **14,** 249-268. (2000).

27. Gundersen, J.K. & Jorgensen, B.B. Microstructure of diffusive boundary layers and the oxygen uptake of the seafloor. Nature 345. 604-607. (1993).

28. Papineau, D., Global Biogeochemical Changes at Both Ends of the Proterozoic: Insights from Phosphorites. *Astrobiology* **10,** 165-181 (2010).

29. Algeo, T.J. & Ingall, E. Sedimentary Corg:P ratios, paleocean ventilation, and Phanerozoic atmospheric pO2. *Palaeogeography, Palaeoclimatology, Palaeoecology* **256,** 130-155 (2007).

30. Partin, C.A., Bekker, A., Planavsky N.J., Scott, C.T, Gill, B.C., Li, C., Podkovyrow, V, Maslov, A., Konhauser, K.O., Lalonde, S.V., Love, G.D, Poulton, S.W. & Lyons, T.W. "Large scale fluctuations in Precambrian atmospheric and oceanic oxygen levels from the record of U in shales". Earth. Plan. Sci. Lett. 369-370, 284-293. (2013).

Acknowledgements

RAB, TML & GSZ gratefully acknowledge funding from the National Environment Research Council (NE/I005978/1). TWD was sponsored from the Inge Lehmann Scholarship and the VILLUM Foundation (VKR023127). MZ is funded by the National Basic Research Program of China (2013CB835000) and the National Natural Science Foundation of China (40930211). AWD was supported by the SFB754 funded by the German DFG (www.sfb754.de).

Author contributions

RAB developed the hypothesis including ideas from all co-authors. TWD provided data. RAB modified the original model of TML. RAB wrote the paper with input from all co-authors. Correspondence and requests for materials should be addressed to

rboyle@biology.sdu.dk

Figure Legends

Figure 1. Redox proxy data is consistent with decreased oxygenation of the marine environment following the early Cambrian increase in bioturbation.

a-b. Bioturbation data from Mangano & Buatois, 2014[3]. Bioturbation index[22,3] refers to % of the original sediment fabric exhibiting disturbance by bioturbation: 0=0%, 1=1–4%, 2=5–30%, 3=31–60%, 4=61–90%, 5=91–99%, 6=100%. **c.** Molybdenum isotope compositions $\delta^{98}Mo = [(^{98}Mo/^{95}Mo)_{sample} / (^{98}Mo/^{95}Mo)_{NIST\text{-}SRM3134} - 1] \cdot 1000$ [‰]. Seawater $\delta^{98}Mo$ scales positively with ocean oxygenation. The maximum $d^{98}Mo$ value (rather than the mean) is the strongest indicator of the extent of ocean oxygenation, because mildly euxinic shales have a lower $d^{98}Mo$ than ambient seawater. **d.** Mo/Total organic carbon (TOC), **e.** U/TOC and **f.** sedimentary Mo and U contents. Both Mo and U are soluble in oxic waters and more efficiently removed under anoxic and sulphidic conditions. Normalisation to TOC scales out the dependence of trace metal enrichment on total organic carbon content. Anoxic settings identified by Fe:Al>0.5, euxinic settings by $Fe_{(Highly\ reactive/total)} > 0.38$ and $Fe_{(pyritised/highly\ reactive)} > 0.7$ (see table S3 for further details and full references). Arrows mark intervals of proposed relative oxygen decline.

Figure 2. Modelled steady-states oxygen/phosphorus reservoir sizes as a function of bioturbation. Steady state size of the atmosphere/surface oxygen (blue, left) and marine phosphorus (green, right) reservoirs for different bulk weathering forcings *W=0.5* (a,b), *W=1.0* (c,d), *W=1.5*(e,f) times the present value and different values for the organic carbon to phosphorus ratio for bioturbated $C{:}P_{biot}$ and laminated $C{:}P_{lam}$ sediments (different lines on each plot).

Figure 3. Examples of dynamic model response to the introduction of oxygen-sensitive bioturbation. Model initialised at a steady state with negligible bioturbation, $f_{biot} = 0.01$,

then dynamic bioturbation $f_{biot} = 1 - anox$ (where *anox* is the ocean anoxic fraction) is introduced 25 million years into each 100 million year simulation. For each model run the upper panel shows the marine reservoirs (relative to their modern values) and relevant fluxes. The lower panel shows the fluxes affecting the phosphorus reservoir (in absolute values of10^{10} mol yr^{-1}). Top two rows show a moderate difference in prescribed C:P burial ratios $C:P_{biot} = 150, C:P_{lam} = 300$ ((a,b), (c,d) and (e,f)), lower two rows a larger difference $C:P_{biot} = 200, C:P_{lam} = 700$ ((g,h), (i,j), (k,l). Columns show different bulk weathering values *W=0.5* ((a,b) and (g,h)), *W=1.0* ((c,d) and (i,j), *W=1.5* ((e,f) and(k,l) left through right. *Abbreviations: PO_4=marine phosphate reservoir, O_2=atmosphere/surface ocean oxygen reservoir, f_{biot}=bioturbated fraction of buried organic matter, newp=new production, anox=ocean anoxic fraction, mocb=marine organic carbon burial, mopb=marine organic phosphorus burial, capb=calcium-bound phosphate burial, fepb=iron adbsorbed phosphate burial, phosw=phosphorus weathering.*

Figure 4. Net change in steady-state oxygen and phosphate reservoirs due to the introduction of dynamical oxygen-sensitive bioturbation. The model was allowed to reach steady-state with negligible bioturbation, then dynamical bioturbation was introduced leading to a new steady-state (i.e. every point in figure 4 corresponds to a dynamical run as equivalent to figure 3). Pre-bioturbation reservoir sizes were subtracted from their respective post-bioturbation values, and the difference is expressed relative to the present-day reservoir size, i.e. $\frac{O_{2(after)} - O_{2(before)}}{O_{20}}$ and $\frac{PO_{4(after)} - PO_{4(before)}}{PO_{40}}$. Results are shown as a function of bulk weathering rate (x-axis) and C:P burial ratio parameter choices (different lines, see legend). **a.** Change in atmosphere-surface-ocean oxygen reservoir. **b.** Change in marine phosphate reservoir.

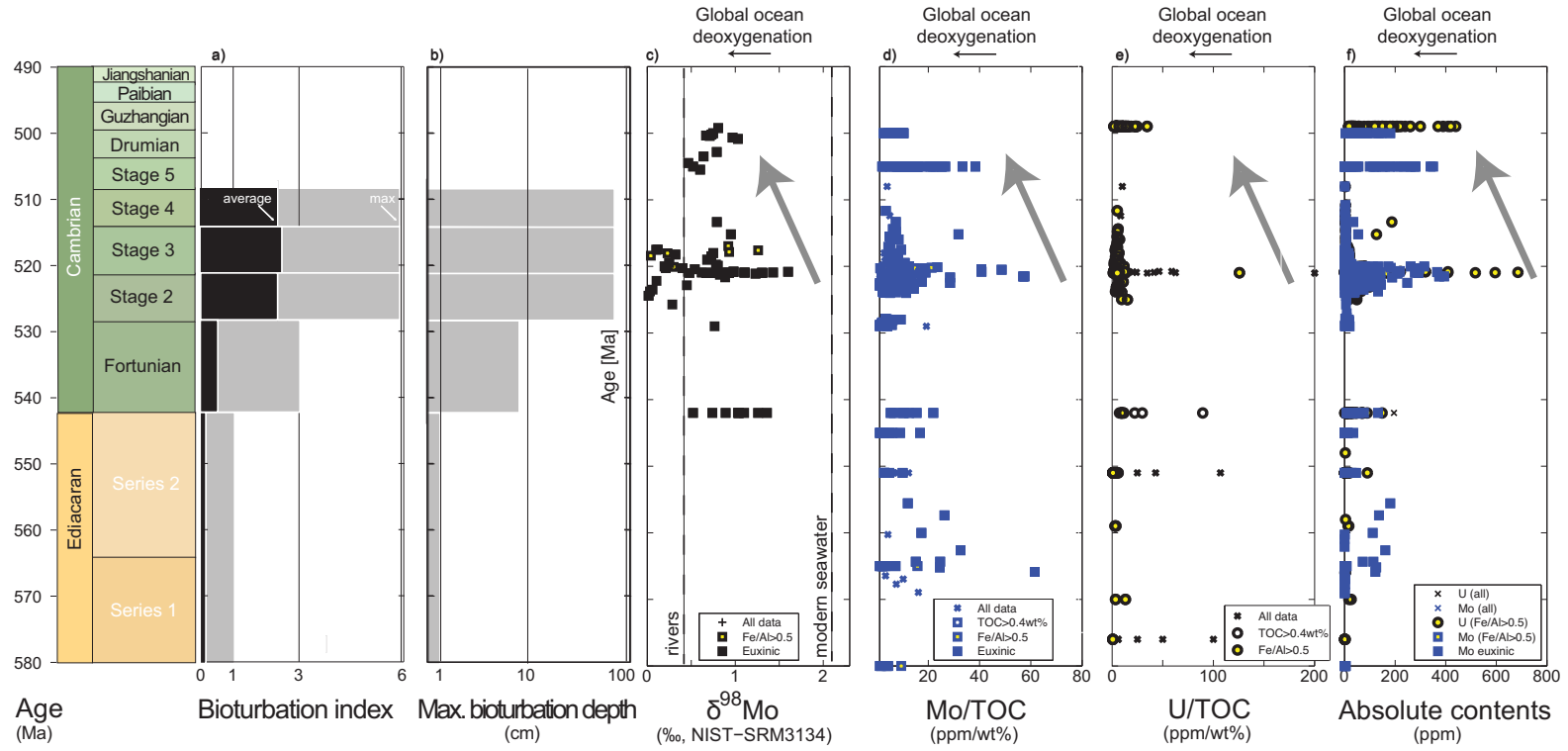
Global ocean deoxygenation
a)
b)
c)
d)
e)
f)
Cambrian
Ediacaran
Jiangshanian
Paibian
Guzhangian
Drumian
Stage 5
Stage 4
Stage 3
Stage 2
Fortunian
Series 2
Series 1
average
max
Age [Ma]
rivers
modern seawater
All data
Fe/Al>0.5
Euxinic
TOC>0.4wt%
U (all)
Mo (all)
U (Fe/Al>0.5)
Mo (Fe/Al>0.5)
Mo euxinic
Age (Ma)
Bioturbation index
Max. bioturbation depth (cm)
δ98Mo (‰, NIST−SRM3134)
Mo/TOC (ppm/wt%)
U/TOC (ppm/wt%)
Absolute contents (ppm)

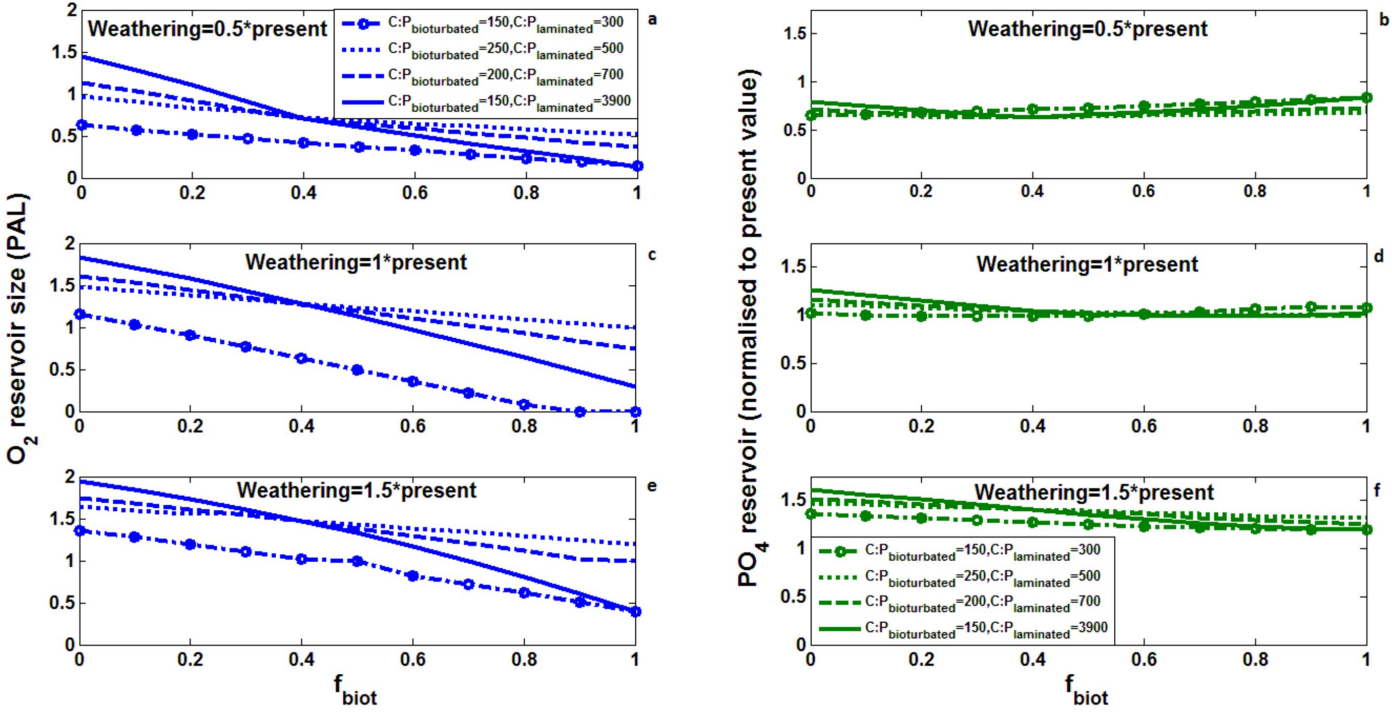
Weathering=0.5*present
a
C:P_bioturbated=150,C:P_laminated=300
C:P_bioturbated=250,C:P_laminated=500
C:P_bioturbated=200,C:P_laminated=700
C:P_bioturbated=150,C:P_laminated=3900
Weathering=1*present
c
Weathering=1.5*present
e
O2 reservoir size (PAL)
f_biot
Weathering=0.5*present
b
Weathering=1*present
d
Weathering=1.5*present
f
PO4 reservoir (normalised to present value)
f_biot

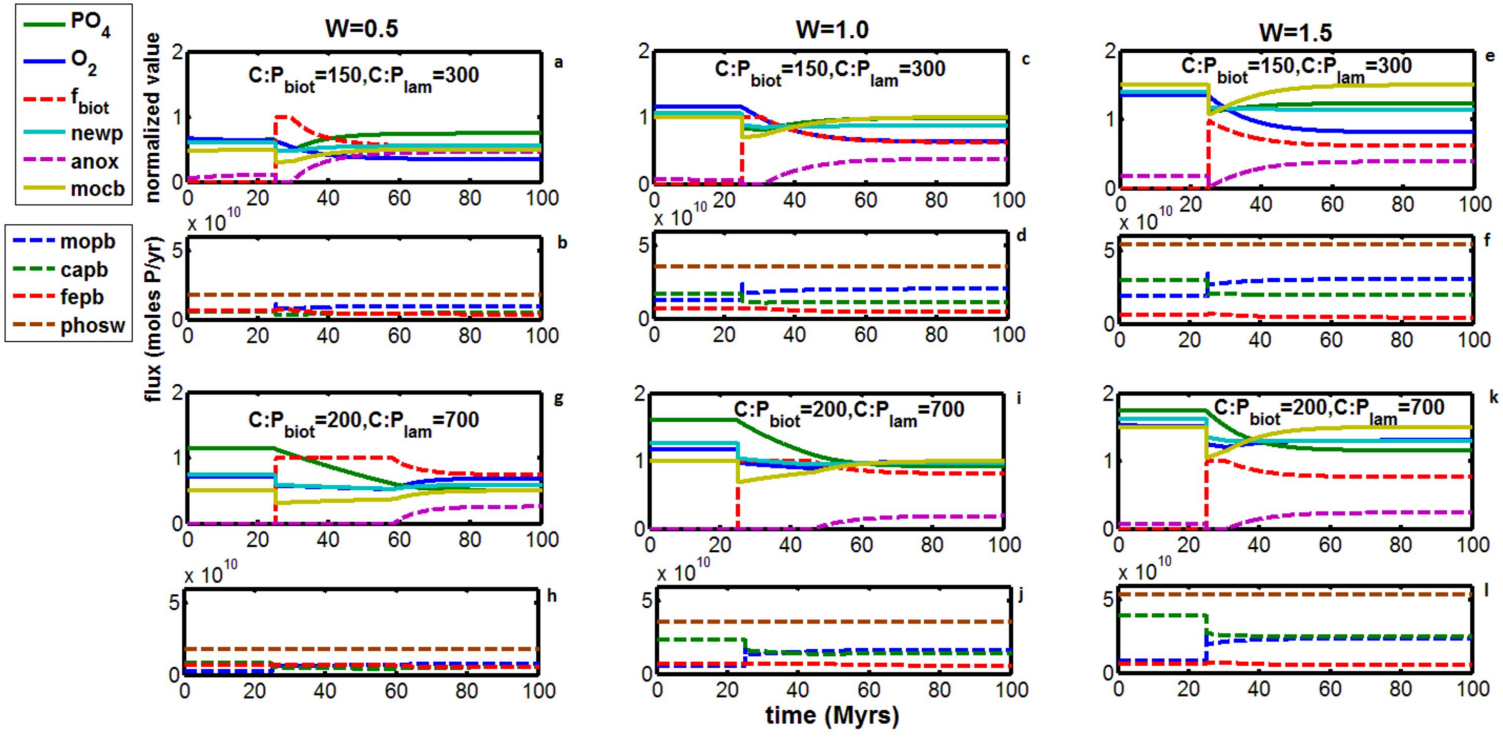
PO4
O2
fbiot
newp
anox
mocb
mopb
capb
fepb
phosw
W=0.5
W=1.0
W=1.5
normalized value
flux (moles P/yr)
x 10^10
C:Pbiot=150,C:Plam=300
C:Pbiot=200,C:Plam=700
a
b
c
d
e
f
g
h
i
j
k
l
time (Myrs)

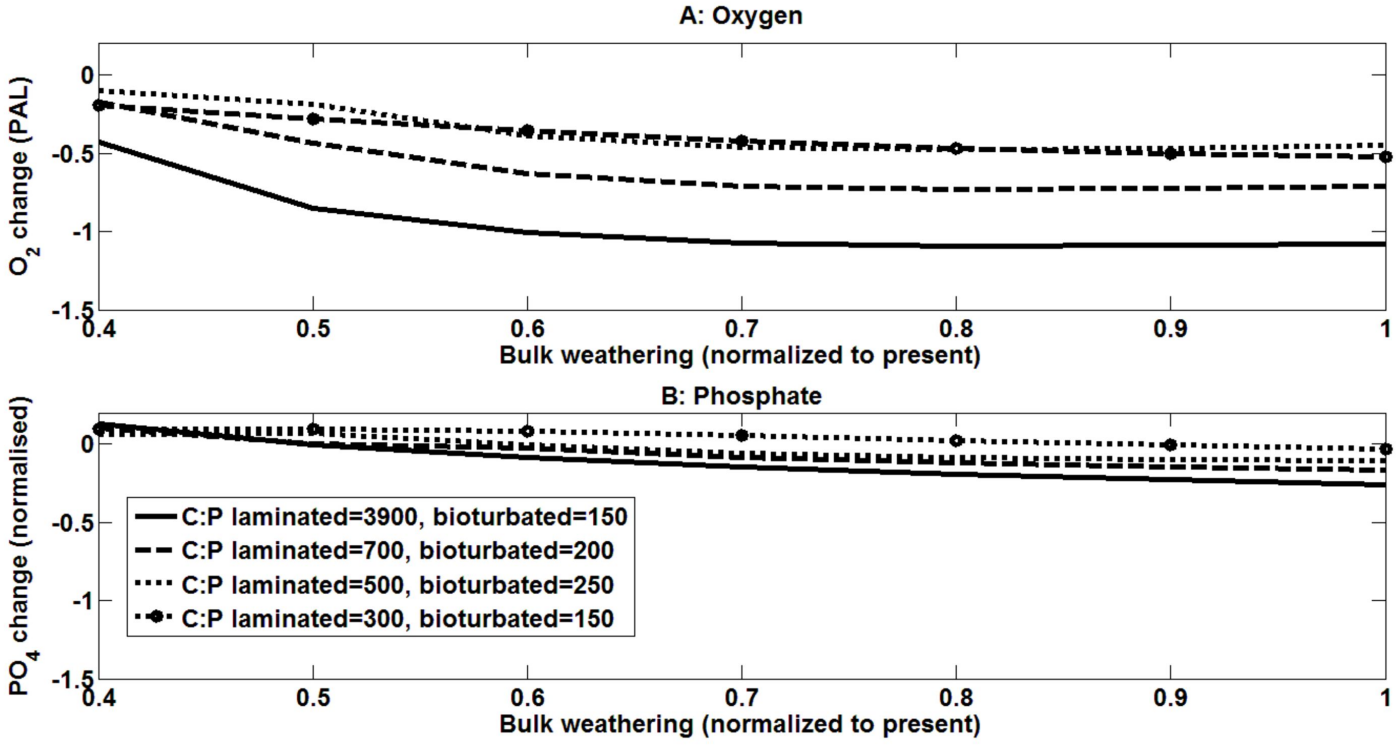
A: Oxygen
O_2 change (PAL)
0
-0.5
-1
-1.5
0.4
0.5
0.6
0.7
0.8
0.9
1
Bulk weathering (normalized to present)
B: Phosphate
PO_4 change (normalised)
0
-0.5
-1
-1.5
0.4
0.5
0.6
0.7
0.8
0.9
1
Bulk weathering (normalized to present)
C:P laminated=3900, bioturbated=150
C:P laminated=700, bioturbated=200
C:P laminated=500, bioturbated=250
C:P laminated=300, bioturbated=150

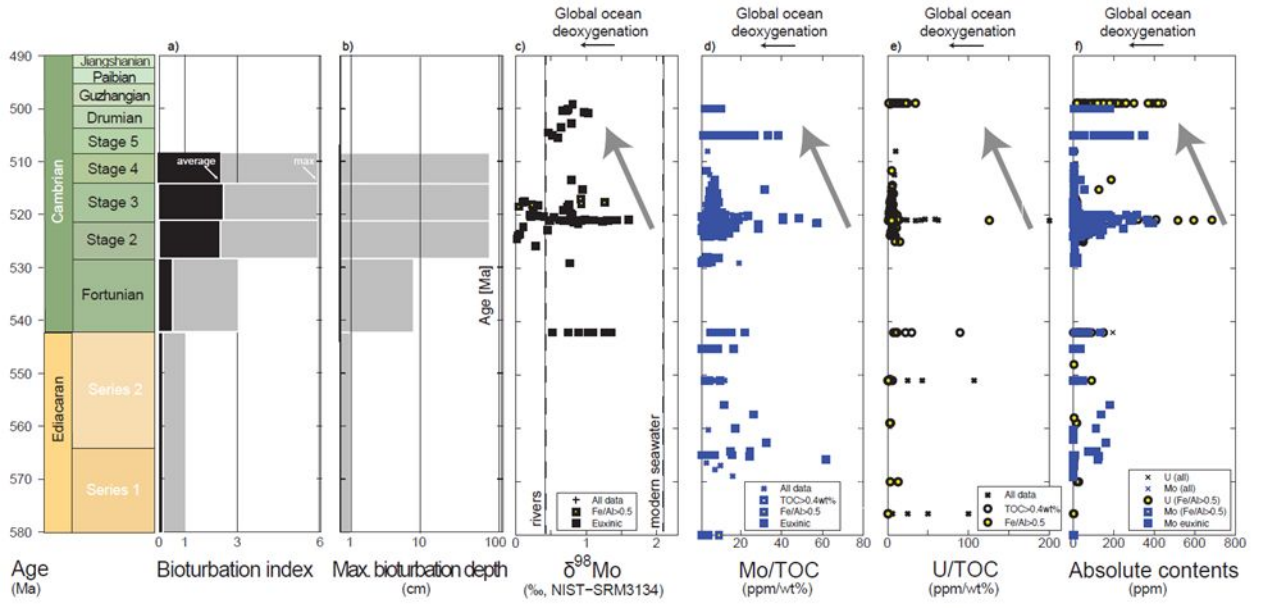
Global ocean deoxygenation
a)
b)
c)
d)
e)
f)
Cambrian
Ediacaran
Jiangshanian
Paibian
Guzhangian
Drumian
Stage 5
Stage 4
Stage 3
Stage 2
Fortunian
Series 2
Series 1
average
max
Age [Ma]
rivers
modern seawater
All data
Fe/Al>0.5
Euxinic
TOC>0.4wt%
U (all)
Mo (all)
U (Fe/Al>0.5)
Mo (Fe/Al>0.5)
Mo euxinic
Age (Ma)
Bioturbation index
Max. bioturbation depth (cm)
δ98Mo (‰, NIST-SRM3134)
Mo/TOC (ppm/wt%)
U/TOC (ppm/wt%)
Absolute contents (ppm)

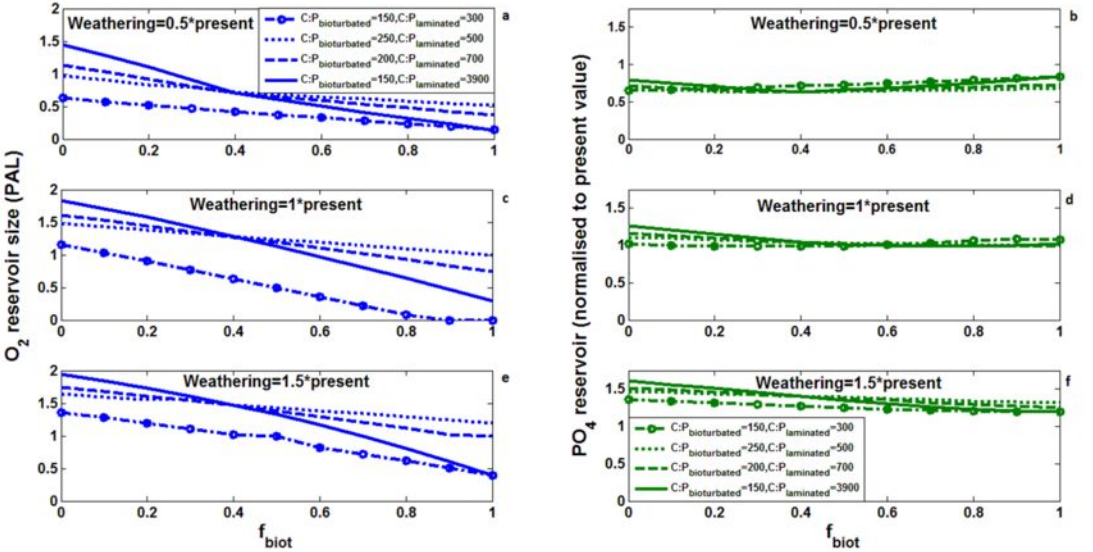
Weathering=0.5*present
a
C:P bioturbated=150,C:P laminated=300
C:P bioturbated=250,C:P laminated=500
C:P bioturbated=200,C:P laminated=700
C:P bioturbated=150,C:P laminated=3900
Weathering=1*present
c
Weathering=1.5*present
e
O2 reservoir size (PAL)
fbiot
Weathering=0.5*present
b
Weathering=1*present
d
Weathering=1.5*present
f
PO4 reservoir (normalised to present value)
fbiot

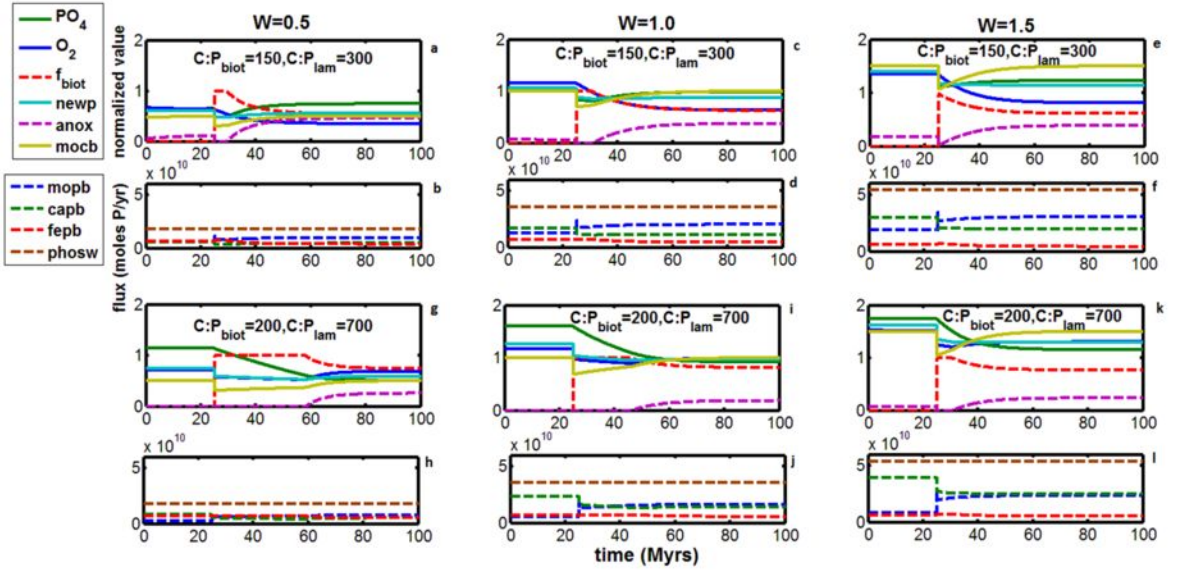
PO4
O2
fbiot
newp
anox
mocb
mopb
capb
fepb
phosw
W=0.5
W=1.0
W=1.5
normalized value
flux (moles P/yr)
C:Pbiot=150,C:Plam=300
C:Pbiot=200,C:Plam=700
x 10^10
a
b
c
d
e
f
g
h
i
j
k
l
time (Myrs)

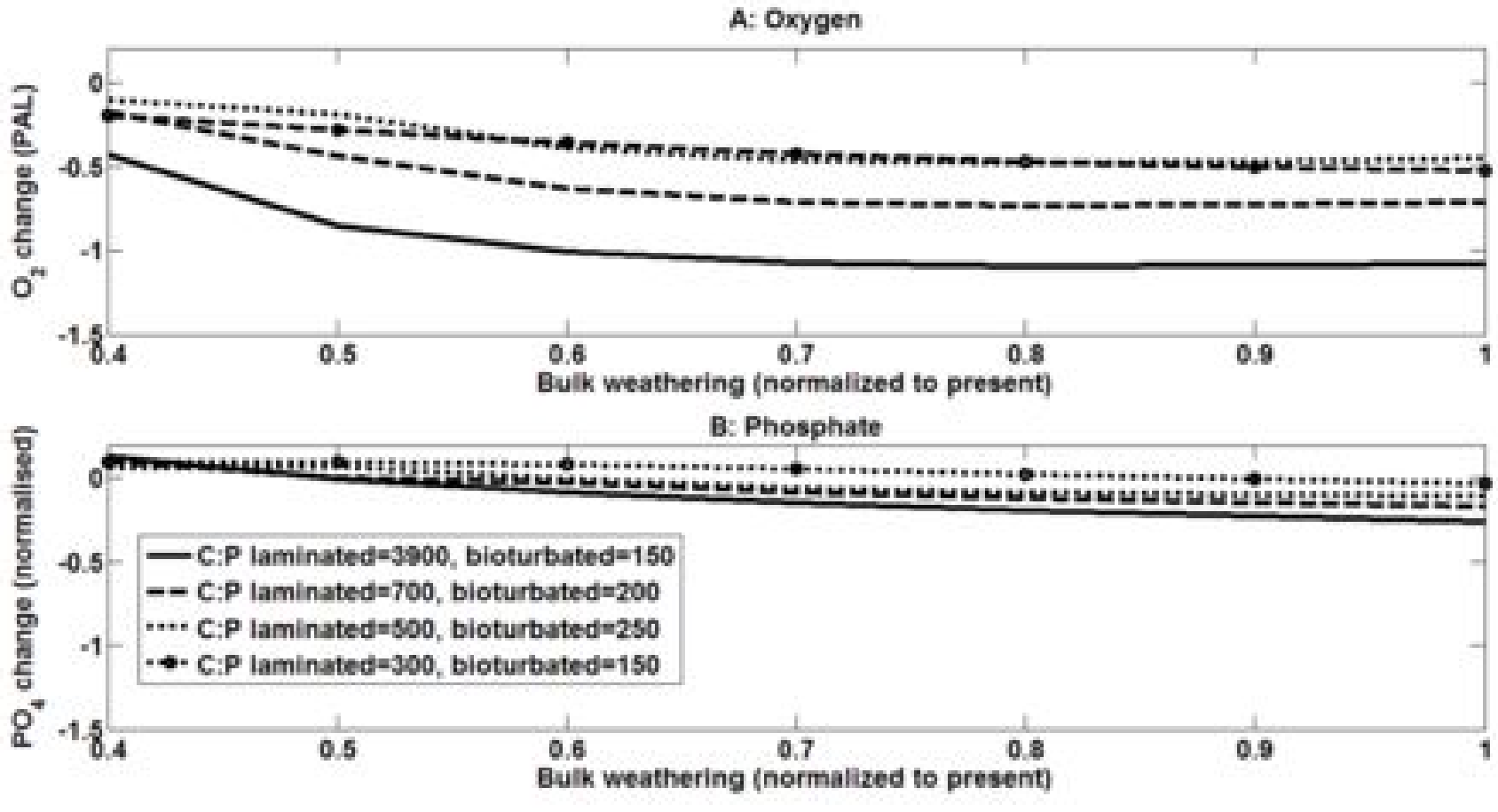
A: Oxygen
O_2 change (PAL)
0
-0.5
-1
-1.5
0.4
0.5
0.6
0.7
0.8
0.9
1
Bulk weathering (normalized to present)
B: Phosphate
PO_4 change (normalised)
0
-0.5
-1
-1.5
0.4
0.5
0.6
0.7
0.8
0.9
1
Bulk weathering (normalized to present)
C:P laminated=3900, bioturbated=150
C:P laminated=700, bioturbated=200
C:P laminated=500, bioturbated=250
C:P laminated=300, bioturbated=150